GEOPHYSICAL RESEARCH LETTERS, VOL. 36, L03102, doi:10.1029/2008GL036036, 2009

Improving retrieval of volcanic sulfur dioxide from backscattered UV satellite observations

Kai Yang,[1,2] Nickolay A. Krotkov,[1,2] Arlin J. Krueger,[3] Simon A. Carn[3,4]
Pawan K. Bhartia,[2] and Pieternel F. Levelt[5]

Received 16 September 2008; revised 8 December 2008; accepted 30 December 2008; published 4 February 2009.

[1] Existing algorithms that use satellite measurements of solar backscattered ultraviolet (BUV) radiances to retrieve sulfur dioxide (SO_2) vertical columns underestimate the large SO_2 amounts encountered in fresh volcanic eruption clouds. To eliminate this underestimation we have developed a new technique, named the Iterative Spectral Fitting (ISF) algorithm, for accurate retrieval of SO_2 vertical columns in the full range of volcanic emissions. The ISF algorithm is applied to Ozone Monitoring Instrument (OMI) BUV measurements of the Sierra Negra eruption (Galàpagos Islands, Ecuador) in October 2005. The results represent major improvements over the operational OMI SO_2 products. Based on the ISF data, we report the largest SO_2 vertical column amount (>1000 Dobson Units (DU), where 1 DU = 2.69×10^{16} molecules/cm^2) ever observed by a space borne instrument, implying that very high concentrations of SO_2 can occur in the lower troposphere during effusive eruptions. **Citation:** Yang, K., N. A. Krotkov, A. J. Krueger, S. A. Carn, P. K. Bhartia, and P. F. Levelt (2009), Improving retrieval of volcanic sulfur dioxide from backscattered UV satellite observations, *Geophys. Res. Lett.*, *36*, L03102, doi:10.1029/2008GL036036.

1. Introduction

[2] Volcanic activity releases various gases and sometimes ash into the atmosphere. These emissions vary in composition, amount, duration, and height, depending on the volcano and the type and intensity of activity. Sulfur dioxide (SO_2) is one of the dominant gases released by volcanic eruptions. Its subsequent dispersion, transport, and conversion to sulfate aerosol may lead to acid rain and air pollution. Large explosive eruptions can inject tremendous amounts of SO_2 and ash into the upper troposphere and stratosphere in a short period of time. While volcanic ash presents severe hazards to aviation safety, it usually does not lead to a significant reduction of solar radiation received at the Earth surface due to rapid fallout. On the other hand, massive amounts of SO_2 that reach the stratosphere are eventually converted to sulfate aerosol which can have lasting impacts, such as reduced global surface temperatures and depletion of stratospheric ozone [*McCormick et al.*, 1995]. Even non-explosive eruptions that emit little ash might have severe regional climate effects if the amount of SO_2 released into the troposphere is large enough, as exemplified by the 1783 Laki (Iceland) eruption that lasted 8–9 months and led to large scale crop failure and livestock loss and the deaths of 24% of the population in Iceland [*Sigurdsson*, 1982].

[3] Ever since the first sighting of SO_2 clouds from the 1982 El Chichón eruption by the Nimbus 7 Total Ozone Mapping Spectrometer (TOMS) [*Krueger*, 1983], satellite measurements have played an indispensable role in assessing and quantifying volcanic emissions, which would be otherwise impossible to monitor globally due to the large size of volcanic eruption clouds, the sporadic nature of volcanic activity and the remote locations of many volcanoes. A unique long-term record of volcanic SO_2 emissions has been compiled from the series of TOMS observations [*Carn et al.*, 2003]. This record is being continued and improved using observations from the Ozone Monitoring Instrument (OMI) [*Levelt et al.*, 2006a] on NASA's Aura platform and supplemented by other backscattered ultraviolet (BUV) measurements from the Global Ozone Monitoring Experiment (GOME) [*Burrows et al.*, 1999], Scanning Imaging Absorption Spectrometer for Atmospheric Chartography (SCIAMACHY) [*Bovensmann et al.*, 1999], and GOME-2 [*Munro et al.*, 2006]. A number of algorithms [see *Yang et al.*, 2007, and references therein] have been developed to retrieve SO_2 from discrete or hyper-spectral BUV measurements in the spectral range 308 – 360 nm. The SO_2 vertical columns derived using these algorithms are impacted by the nonlinear effect [*Yang et al.*, 2007], depending on the SO_2 amount and the wavelengths used.

[4] In this paper, we describe OMI operational data (section 2) and a new iterative spectral fitting (ISF) algorithm that performs simultaneous retrievals of ozone and SO_2 with a proper treatment of the nonlinear effect (section 3). We compare operational and ISF results for an effusive eruption of Sierra Negra volcano (Galápagos Islands) in October 2005 to demonstrate that substantial improvements are achieved using the ISF algorithm (section 4).

2. OMI Data

[5] OMI is a Dutch-Finnish built UV/visible spectrometer that has been operating successfully on NASA's Aura spacecraft since its launch in July 2004 [*Levelt et al.*, 2006a]. It has maintained a stable radiometric calibration while making measurements of direct and backscattered solar radiation with hyper-spectral resolution, covering the

[1] Goddard Earth Sciences and Technology Center, University of Maryland Baltimore County, Baltimore, Maryland, USA.
[2] Laboratory of Atmospheres, NASA Goddard Space Flight Center, Greenbelt, Maryland, USA.
[3] Joint Center for Earth Systems Technology, University of Maryland Baltimore County, Baltimore, Maryland, USA.
[4] Now at Department of Geological and Mining Engineering and Sciences, Michigan Technological University, Houghton, Michigan, USA.
[5] Royal Dutch Meteorological Institute, De Bilt, Netherlands.

0094-8276/09/2008GL036036$05.00

globe daily (when in global mode) at a high nadir spatial resolution. The hyper-spectral measurements have facilitated an accurate wavelength calibration [*Caspar and Chance*, 1997; *Liu et al.*, 2005] and the characterization of the spectral response of the instrument [*Liu et al.*, 2005]. The unique combination of OMI observation characteristics has been exploited [*Levelt et al.*, 2006b, and references therein] to improve determination of effective cloud pressures, measurements of aerosol properties, and retrievals of a number of trace gases relevant to climate and air quality, including ozone, NO_2, HCHO, BrO, and SO_2.

[6] For total ozone and SO_2 retrievals, we have used data from the OMI UV-2 channel, which has a nadir footprint of 13×24 km^2 in the spectral range 310 – 380 nm at a sampling rate of ~0.15 nm/pixel and a spectral resolution of ~0.42 nm. This spectral range covers the ozone Huggins band and a large portion of the strong and weak absorption features of the SO_2 band. The measured spectra contain well-distinguished spectral structures of the Ring effect resulting from Rotational Raman Scattering (RRS) [see *Joiner and Vasilkov*, 2006, and references therein] and absorptions of constituent trace gases because of the high sampling rate and narrow spectral resolution of OMI's UV-2 channel, enabling optimal selection of measurements at specific wavelengths to maximize detection sensitivity to low SO_2 loading. Consequently OMI observations have provided unprecedented measurements of SO_2 emissions from anthropogenic and natural sources, and a 150-fold improvement in sensitivity over TOMS SO_2 measurements [*Krotkov et al.*, 2006].

3. Iterative Spectral Fit Algorithm

[7] Two retrieval techniques, the band residual difference (BRD) method [*Krotkov et al.*, 2006] for boundary layer SO_2 and the Linear Fit (LF) algorithm [*Yang et al.*, 2007] for volcanic SO_2, are being used operationally to produce SO_2 vertical columns from OMI UV-2 measurements. The LF algorithm is designed to work with both discrete-wavelength and hyper-spectral measurements and the BRD method can also be extended to include measurements at more wavelengths; thus far they have been applied to measurements at a small set of wavelengths only. Although both techniques have not fully exploited the hyper-spectral capability of OMI, they have successfully measured a wide range of SO_2 loadings encountered in global observations [*Carn et al.*, 2007; *Yang et al.*, 2007; *Krotkov et al.*, 2008], and are fast enough to generate SO_2 products in near real time for aviation hazard mitigation [*Carn et al.*, 2008]. Limitations in retrieval accuracy for large eruptions are expected because these techniques assume an approximate linear relationship between SO_2 column and the residuals at a set of wavelengths [*Yang et al.*, 2007]. Residuals here are calculated as N-value ($N = -100 \log_{10} I$, where I is the sun normalized radiance) differences between the measurements and forward model simulations with an initial guess of zero SO_2. The linear approximation is justified when the amount of SO_2 is small, because the mean path traversing the atmosphere by the measured BUV photons is almost identical to that of the BUV photons in a SO_2-free atmosphere. However with a larger SO_2 amount, the stronger absorption suppresses more subsequent photon scatterings, reducing the relative contribution to the measured radiance by photons that have passed the SO2 medium, leading to an underestimation of the actual SO2 value by the BRD and LF methods. The LF method has a wider valid range than the BRD algorithm primarily because the former uses longer wavelength measurements, where SO_2 absorption is weaker and the linear approximation holds for SO_2 loadings up to ~100 DU [*Yang et al.*, 2007]. For larger SO_2 loadings, the non-linear response of the N-value residuals to the change in SO_2 becomes the main limiting factor of the operational OMI SO_2 algorithms.

[8] To overcome this limitation due to the non-linear effect, the LF equation can be solved iteratively with an updated linearization point and weighting functions at each step. Algebraically, the LF equation for a wavelength band is expressed as

$$N_{obs} - N_i = \Delta\Omega \left.\frac{\partial N}{\partial \Omega}\right|_{\Omega=\Omega_i} + \Delta\Xi \left.\frac{\partial N}{\partial \Xi}\right|_{\Xi=\Xi_i} + p_{rrs}\ \sigma_i^{rrs} + \left(\Delta F_c + \sum_{k=1}^{n=2} c_k(\lambda-\lambda_0)^k\right) \left.\frac{\partial N}{\partial F_c}\right|_{F_c=F_{ci}} + \varepsilon, \quad (1)$$

where N_{obs} is the OMI measured N-value, N_i is the computed N-value at the ith iteration based on a forward model, and ε is the total error for the wavelength band. Starting with an initial guess of ozone (Ω_0) based on the seasonal zonal mean value at the location of the observation and zero SO_2 ($\Xi_0 = 0$), the cloud fraction parameter (F_c) of a Mixed Lambert-Equivalent Reflectivity (MLER) model [*Ahmad et al.*, 2004] is determined at $\lambda_0 = 333$ nm (where ozone and SO_2 absorption cross sections and the RRS effect are small), with MLER cloud pressure determined by the effective cloud pressure from the OMI RRS (OMCLDRR) product [*Joiner and Vasilkov*, 2006]. Note that when the effective scene reflectivity is either low (<0.15, usually under partial cloud conditions or in the presence of non-absorbing aerosols) or very high (>0.8, usually when the surface is covered by snow/ice), the Lambert Equivalent Reflectivity (LER) model is used (i.e., F_c is replaced by LER) so that the forward model can better approximate the mean path of the BUV photons measured by the satellite instrument. The linear set of equations (1) for each wavelength can be solved by least squares fitting of residuals ($N_{obs} - N_i$) to the weighting functions ($\frac{\partial N}{\partial \Omega}$, $\frac{\partial N}{\partial \Xi}$, $\frac{\partial N}{\partial F_c}$, $(\lambda-\lambda_0)\frac{\partial N}{\partial F_c}$, $(\lambda-\lambda_0)^2\frac{\partial N}{\partial F_c}$) and the RRS spectrum ($\sigma^{rrs}$) [*Sioris and Evans*, 1999] to obtain state vector adjustments: ΔF_c, polynomial coefficients (c_1 and c_2), RRS scaling parameter (p_{rrs}), and the linearization point for the next iteration ($\Omega_{i+1} = \Omega_i + \Delta\Omega$, $\Xi_{i+1} = \Xi_i + \Delta\Xi$). The weighting functions and the RRS spectrum are updated at each iterative step. The final solution of ozone and SO_2 columns is achieved when the iteration converges, i.e., the changes in ozone and SO_2 between successive iterations are below certain thresholds. The error due to the non-linear effect, which manifests itself in the higher order terms of $\Delta\Omega$ and $\Delta\Xi$ (absorbed into ε in equation (1)), becomes negligible as the iterative process converges.

[9] The TOMRAD forward model, which implements Dave's iterative solution to the vector radiative transfer equation [*Dave*, 1964] with a pseudo-spherical correction [*Caudill et al.*, 1997], is used to calculate the upwelling

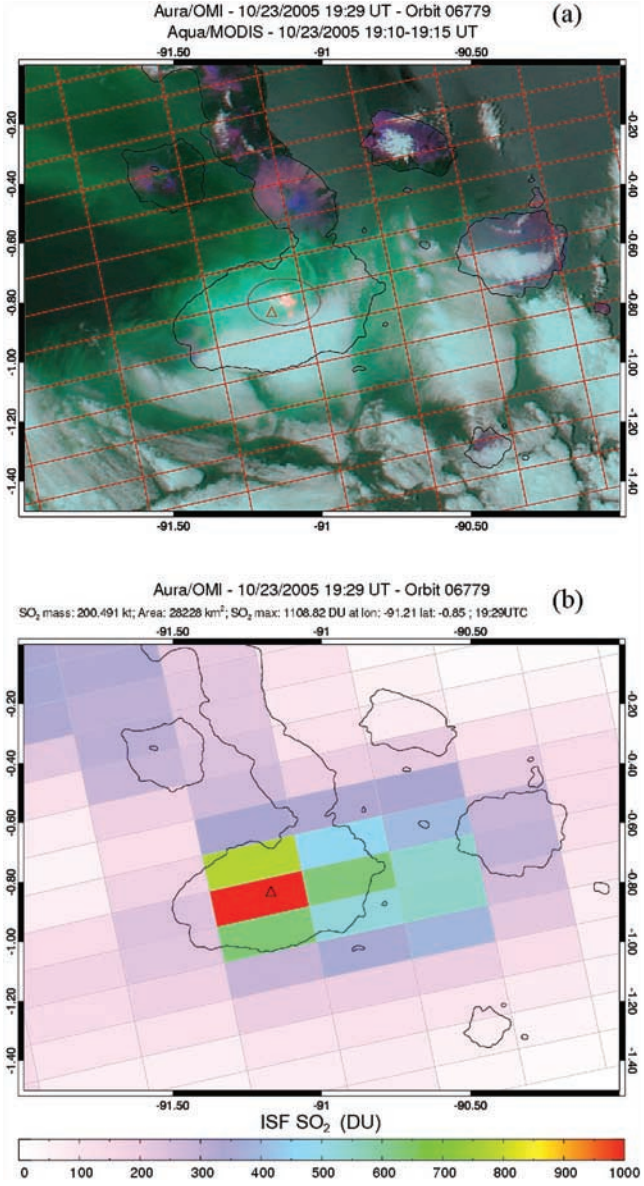

Figure 1. The MODIS instrument on the Aqua satellite observed the Sierra Negra eruption about 15 minutes before OMI on October 23, 2005. (a) A color composite of MODIS bands 7 (2114.1 nm, Red), 2 (856.5 nm, Green), and 1 (645.5 nm, Blue) over the Galápagos Islands and (b) the OMI ISF SO_2 map of the same area. OMI pixel footprints are overlaid on both Figures 1a and 1b. Sierra Negra volcano (denoted by the symbol △ in Figures 1a and 1b) is located at 91.17°W and 0.83°S and rises to an elevation of 1.1 km. Oval outline in Figure 1a encloses the lava flows (orange hot spot) seen by MODIS.

radiance (I) at each wavelength and the corresponding weighting functions. Aerosols are not included in the forward model, but we account for their effects on the radiances implicitly by deriving the MLER cloud fraction or the LER value and treating them as a function of wavelength using a second-order polynomial. The RRS spectrum (σ^{rrs}), also known as the Ring cross section, is calculated using the method developed by *Sioris and Evans* [1999]. This method can take into account the sun-target-observer geometry and the absorber (ozone and SO_2) amounts, which are updated at each iteration step, accurately characterizing the spectral structure of RRS filling-in due to ozone and SO_2 absorption.

4. Case Study: October 2005 Eruption of Sierra Negra

[10] A large eruption started at Sierra Negra volcano (Galápagos Islands) at about 5:30 pm local time on October 22, 2005 [*Geist et al.*, 2008], sending ash and steam clouds high into the atmosphere after the OMI overpass at 1:45 pm local time. These high clouds had drifted away by the next day when OMI made its first observation of this eruption, which became effusive with strong lava fountains (up to 300 m high) that produced long (>2 km) lava flows, manifested as the hot (orange) spot in Figure 1a, a composite Moderate Resolution Imaging Spectroradiometer (MODIS) image. This activity released very little ash but large amounts of gas, including SO_2, into the lower troposphere, providing an excellent test of the ISF technique described in this paper.

[11] We applied the ISF approach described above to the OMI measured spectra in the wavelength range 317.8 – 333 nm, which contains about 100 spectral measurements. This reduces the impact of random noise compared to using just a few discrete wavelengths selected from a full spectrum; consequently information contents can be more precisely retrieved. Since most of the measured TOA photons at these wavelengths have traversed the entire atmosphere, they provide information on total columns of the absorbers, but limited information about their vertical distributions. Therefore a priori profiles for both SO_2 and ozone are employed in our forward model. For ozone, we use the TOMS Version 8 (V8) profile climatology [*Bhartia and Wellemeyer*, 2002], which is uniquely determined by latitude, day of the year, and ozone amount. For the SO_2 plume, we represent its profile using a Gaussian, characterized by a central altitude and width.

[12] We demonstrate here that retrievals of very large total SO_2 columns are greatly improved using the new ISF algorithm. In Figure 2, we compare ISF ozone and SO_2 results with those from the operational OMI LF algorithm [*Yang et al.*, 2007] on October 23, 2005; both algorithms assumed a central plume altitude of ~2.5 km, which is appropriate for this case where SO_2 is mostly confined to the lower troposphere. Field observers on October 23 reported a plume 'only several kilometres high' [*Geist et al.*, 2008]. Figure 2a shows the ozone consistency achieved using the ISF method, with ISF ozone values unaffected by the presence of the SO_2 plume, whereas the operational LF ozone map (Figure 2b) contains artifacts, including high ozone at the plume edge and unrealistically low ozone in the interior of the plume. The internal consistency of the ISF ozone data serves as an indirect validation of the simultaneously retrieved SO_2 columns, which are generally larger than the corresponding LF columns. A slight reduction in retrieved ozone in the small area just over the volcanic vent implies that small ozone errors may be associated with retrievals of extremely large SO_2 columns. However, retrievals with ozone values preset to those outside the plume yield similar SO_2 columns, indicating that these ozone errors have no significant impact on the SO_2 results.

Figure 3 illustrates an approximate linear relationship between LF and ISF SO_2 columns below 100 DU, in agreement with the limitations of the LF method noted in our previous paper [*Yang et al.*, 2007]. Above 100 DU of SO_2, the underestimation of SO_2 by the LF algorithm becomes more severe as the actual SO_2 column increases, and in these cases, ISF retrievals are needed to accurately retrieve the vertical columns. For the Sierra Negra eruption on October 23, 2005, the highest retrieved SO_2 column is located directly above the eruptive vent (see Figure 1b), with an ISF column exceeding 1100 DU. To our knowledge this is the largest SO_2 vertical column retrieved to date by a space borne instrument. For the same pixel, the LF algorithm yields 247 DU, a 78% underestimation. From OMI measurements on this day, the ISF SO_2 tonnage is ~1740 kilotons for the entire plume, nearly twice that (~950 kilotons) obtained using the LF data. The very high SO_2 column amounts directly over or close to the volcanic vent are probably the result of the high SO_2 emission rates associated with strong lava fountains and large lava flows, coupled with the small OMI footprint and slow dispersion of the volcanic plume due to light winds (wind speed ~3 m/s) at the time of the OMI observation.

5. Conclusions

[13] For strong volcanic eruptions that inject large amounts of SO_2 into the atmosphere, accurate quantification of the emissions from satellite BUV measurements requires proper accounting for the non-linear SO_2 absorption effect, and this can be accomplished using the ISF technique described in this paper. Application of the ISF method to OMI observations of the Sierra Negra eruption on October 23, 2005 and comparison with the corresponding operational OMI SO2 retrievals using the LF algorithm clearly demonstrate great improvements in quantification of large SO2 columns above the LF upper valid range of ~100 DU. The iterative retrieval approach described here can be modified to use discrete wavelength measurements, such as those from the series of TOMS instruments, offering the potential to improve the long-term SO_2 emission record. Future work will include further improvement of the retrieval of volcanic SO_2 columns by deriving plume altitudes directly from BUV measurements.

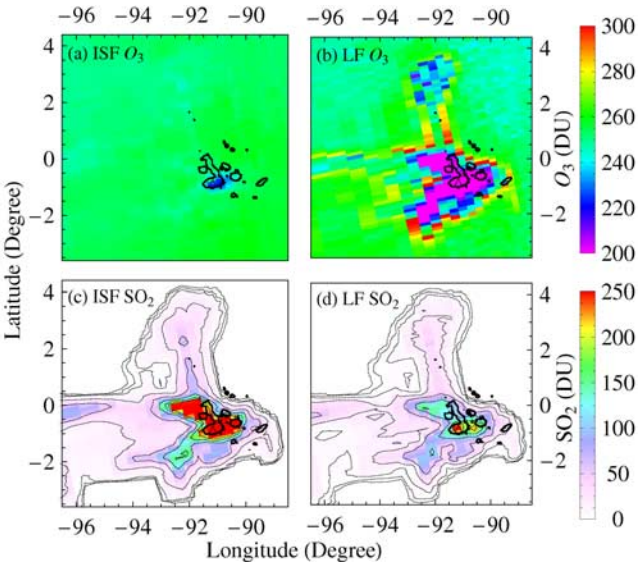

Figure 2. OMI ozone and SO_2 maps derived from OMI BUV radiances for the Sierra Negra volcanic cloud on October 23, 2005, using the ISF, (a) O_3 and (c) SO_2, and LF, (b) O_3 and (d) SO_2, algorithms assuming a fixed SO_2 plume central altitude of 2.5 km and a plume width of 3.5 km (defined as the full width at half maximum of the Gaussian profile) for ISF and a width of ~5 km (i.e., the width of Umkehr layer 0) for LF.

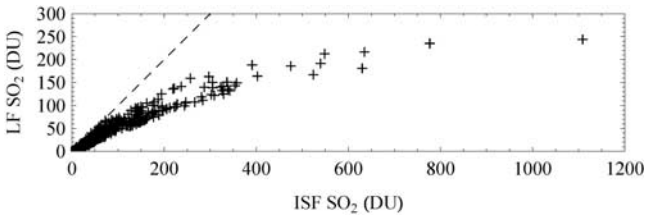

Figure 3. Comparison of ISF and LF SO_2 columns in the Sierra Negra eruption cloud on October 23, 2005. The LF retrievals saturate at about 200 DU in this case.

[14] **Acknowledgments.** This work was supported in part by NASA under grant NNS06AA05G (NASA volcanic cloud data for aviation hazards) and by the U.S. OMI Science Team.

References

Ahmad, Z., P. K. Bhartia, and N. Krotkov (2004), Spectral properties of backscattered UV radiation in cloudy atmospheres, *J. Geophys. Res.*, *109*, D01201, doi:10.1029/2003JD003395.

Bhartia, P. K., and C. W. Wellemeyer (2002), TOMS-V8 Total O3 Algorithm, in *Algorithm Theoretical Baseline Document, vol. II, OMI Ozone Products*, edited by P. K. Bhartia, pp. 15–31, NASA Goddard Earth Sci. Data and Inf. Serv. Cent., Greenbelt, Md., (Available at http://eospso.gsfc.nasa.gov/eos_homepage/for_scientists/atbd/docs/OMI/ATBD-OMI-02.pdf).

Bovensmann, H., J. P. Burrows, M. Buchwitz, J. Frerick, S. Nol, V. V. Rozanov, K. V. Chance, and A. P. H. Goede (1999), SCIAMACHY: Mission objectives and measurement modes, *J. Atmos. Sci.*, *56*, 127–150.

Burrows, J. P., et al. (1999), The Global Ozone Monitoring Experiment (GOME): Mission concept and first scientific results, *J. Atmos. Sci.*, *56*, 151–175.

Carn, S. A., A. J. Krueger, G. J. S. Bluth, S. J. Schaefer, N. A. Krotkov, I. M. Watson, and S. Datta (2003), Volcanic eruption detection by the Total Ozone Mapping Spectrometer (TOMS) instruments: A 22-year record of sulphur dioxide and ash emissions, in *Volcanic Degassing*, edited by C. Oppenheimer, D. M. Pyle, and J. Barclay, *Spec. Publ. Geol. Soc. London*, *213*, 177–202.

Carn, S. A., A. J. Krueger, N. A. Krotkov, K. Yang, and P. F. Levelt (2007), Sulfur dioxide emissions from Peruvian copper smelters detected by the Ozone Monitoring Instrument, *Geophys. Res. Lett.*, *34*, L09801, doi:10.1029/2006GL029020.

Carn, S. A., A. J. Krueger, N. A. Krotkov, K. Yang, and K. Evans (2008), Tracking volcanic sulfur dioxide clouds for aviation hazard mitigation, *Nat. Hazards*, doi:10.1007/s11069-008-9228-4.

Caspar, C, and K. Chance (1997), GOME wavelength calibration using solar and atmospheric spectra, in *Third ERS Symposium on Space at the Service of our Environment: Florence, Italy, 14–21 March 1997*, edited by T.-D. Guyenne and D. Danesy, ESA Publ. Div., Noordwijk, Netherlands.

Caudill, T. R., D. E. Flittner, B. M. Herman, O. Torres, and R. D. McPeters (1997), Evaluation of the pseudo-spherical approximation for backscattered ultraviolet radiances and ozone retrieval, *J. Geophys. Res.*, *102*, 3881–3890.

Dave, J. V. (1964), Meaning of successive iteration of the auxiliary equation of radiative transfer, *Astrophys. J.*, *140*, 1292–1303.

Geist, D. J., K. S. Harpp, T. R. Naumann, M. Poland, W. W. Chadwick, M. Hall, and E. Rader (2008), The 2005 eruption of Sierra Negra volcano, Galápagos, Ecuador, *Bull. Volcanol.*, *70*, 655–673.

Joiner, J., and A. P. Vasilkov (2006), First results from the OMI rotational Raman scattering cloud pressure algorithm, *IEEE Trans. Geosci. Remote Sens.*, *44*, 1272–1282.

Krotkov, N. A., S. A. Carn, A. J. Krueger, P. K. Bhartia, and K. Yang (2006), Band residual difference algorithm for retrieval of SO_2 from the Aura Ozone Monitoring Instrument (OMI), *IEEE Trans. Geosci. Remote Sens.*, *44*(5), 1259–1266, doi:10.1109/TGRS.2005.861932.

Krotkov, N. A., et al. (2008), Validation of SO_2 retrievals from the Ozone Monitoring Instrument over NE China, *J. Geophys. Res.*, *113*, D16S40, doi:10.1029/2007JD008818.

Krueger, A. J. (1983), Sighting of El Chichon sulfur dioxide clouds with the Nimbus 7 Total Ozone Mapping Spectrometer, *Science*, *220*, 1377–1379, doi:10.1126/science.220.4604.1377.

Levelt, P. F., G. H. J. van den Oord, M. R. Dobber, A. Malkki, H. Visser, J. de Vries, P. Stammes, J. Lundell, and H. Saari (2006a), The Ozone Monitoring Instrument, *IEEE Trans. Geosci. Remote Sens.*, *44*, 1093–1101, doi:10.1109/TGRS.2006.872333.

Levelt, P. F., E. Hilsenrath, G. W. Leppelmeier, G. H. J. van den Oord, P. K. Bhartia, J. Tamminen, J. F. de Haan, and J. P. Veefkind (2006b), Science objectives of the Ozone Monitoring Instrument, *IEEE Trans. Geosci. Remote Sens.*, *44*, 1199–1208, doi:10.1109/TGRS.2006.872336.

Liu, X., K. Chance, C. E. Sioris, R. J. D. Spurr, T. P. Kurosu, R. V. Martin, and M. J. Newchurch (2005), Ozone profile and tropospheric ozone retrievals from the Global Ozone Monitoring Experiment: Algorithm description and validation, *J. Geophys. Res.*, *110*, D20307, doi:10.1029/2005JD006240.

McCormick, M. P., L. W. Thomason, and C. R. Trepte (1995), Atmospheric effects of the Mt. Pinatubo eruption, *Nature*, *373*, 399–404.

Munro, R., et al. (2006), GOME-2 on MetOp, in *The 2006 EUMETSAT Meteorological Satellite Conference (CD-ROM), EUMETSAT Publ. 48*, Eur. Org. for the Exploit. of Meteorol. Sat., Darmstadt, Germany, (Available at http://www.eumetsat.int/Home/Main/Publications/Conference_and_Workshop_Proceedings/groups/cps/documents/document/pdf_conf_p48_s4_01_munro_v.pdf).

Sigurdsson, H. (1982), Volcanic pollution and climate: The 1783 Laki eruption, *Eos Trans. AGU*, *10*, 601–602.

Sioris, C. E., and W. F. J. Evans (1999), Filling in of Fraunhofer and gas-absorption lines in sky spectra as caused by rotational Raman scattering, *Appl. Opt.*, *38*, 2706–2713.

Yang, K., N. A. Krotkov, A. J. Krueger, S. A. Carn, P. K. Bhartia, and P. F. Levelt (2007), Retrieval of large volcanic SO_2 columns from the Aura Ozone Monitoring Instrument: Comparison and limitations, *J. Geophys. Res.*, *112*, D24S43, doi:10.1029/2007JD008825.

P. K. Bhartia, N. A. Krotkov, and K. Yang, NASA Goddard Space Flight Center, Mail Code 613.3, Greenbelt, MD 20771, USA. (kai.yang-1@nasa.gov)

S. A. Carn, Department of Geological and Mining Engineering and Sciences, Michigan Technological University, Houghton, MI 49931–1295, USA.

A. J. Krueger, Joint Center for Earth Systems Technology, University of Maryland Baltimore County, Baltimore, MD 21250, USA.

P. F. Levelt, Royal Dutch Meteorological Institute, P.O. Box 201, NL-3730 AE De Bilt, Netherlands.